Analysis & Sensing

Research Article
doi.org/10.1002/anse.202400025

Chemistry Europe
European Chemical Societies Publishing

www.analysis-sensing.org

Unimolecular Cucurbit[7]uril-Based Indicator Displacement Assay with Dual Signal-Readout for the Detection of Drugs

Pierre Picchetti,*[a] Maria Vittoria Balli,[b] Seth Baker,[c] Nilima Manoj Kumar,[a] Patrick Gruhs,[a] Luca Prodi,[b] and Frank Biedermann*[a]

Point-of-care diagnostics relies on optical and electrochemical sensors to develop devices that are both compact and cost-effective. Therefore, the search for new design principles for chemosensors that enable multiple signal outputs is a particularly interesting concept. In this work, we present an unimolecular chemosensor based on cucurbit[7]uril that combines two signal readouts - namely fluorescent and electrochemical signals - in a single chemosensor design. This is achieved by utilizing the tunable fluorescence and the electrochemical properties of the reporter molecule, which depend on whether or not it is engulfed by the cucurbit[7]uril cavity in the absence or presence of the analyte. By setting up an assay using the dual readout chemosensor, illicit drug formulations containing pancuronium bromide or nicotine can be detected at low micromolar concentrations (0–100 μM). This assay is compatible with standard fluorescence plate readers and electrochemical devices, including commercially available screen-printed electrodes. Overall, the chemosensor presented in this study represents a significant advance in the development of cucurbit[7]uril chemosensors, characterized by multimodal detection capabilities. It uniquely combines traditional optical and electrochemical detection methods in a single molecular design.

Introduction

Synthetic macrocyclic receptors such as cryptands,[1] cavitands,[2] calix[n]arenes,[3] pillar[n]arenes,[4] or cucurbit[n]urils[5] (CBn) have shown much potential for the development of chemosensor ensembles, hereafter referred to as chemosensors, for molecular diagnostics.[6] It is generally anticipated that these chemosensors if successfully translated into macroscopic sensory devices, will provide cost-effective and user-friendly alternatives to conventional clinical testing that relies on mass spectrometry (MS) and high-performance liquid chromatography (HPLC).

Among the macrocyclic hosts to be used as chemosensors, CB*n* are characterized by their exceptionally high binding affinity to biologically relevant analytes, including metabolites and neurotransmitters.[6b,7] For example, by setting up a competitive binding assay,[8] CB*n* chemosensors have been successfully applied for the luminescence-based detection of biomolecules and drugs,[8a,9] and for bioimaging applications.[10] In addition, ongoing efforts are focused on improving the stability of CB*n*-based chemosensors in complex biofluids. These include the recent development of a cucurbit[8]uril-based rotaxane design[11] and the use of cucurbit[7]uril (CB7) based unimolecular chemosensors in which the indicator dye is covalently attached to the outer rim of the macrocycle via a flexible linker.[12]

Existing CB*n*-based chemosensors rely mainly on an optical signal readout. However, the development of CB*n* chemosensors with multimodal signal readout, which goes beyond purely optical detection, will offer considerable advantages. For example, chemosensors that exhibit both luminescence and electrochemical detection would be particularly useful given the rise of miniaturized optical and electrochemical technologies in portable devices and for point-of-care diagnostics.[13] At present, however, the realization of such dual-readout CB*n*-based chemosensors has not yet been achieved.

Early studies by Kaifer, Ong, Kim, and Inue[14] demonstrated how the formation of CB*n*•guest complexes modulates the electrochemical properties of electroactive guest, such as a shift in redox potential and a change in current intensity, depending on whether the redox-active guest is bound to the macrocycle or not. Since then, however, only a limited number of electrochemical CB*n* sensors have been developed to detect bioactive molecules that function *via* a competitive binding assay. Wang, Yu, and coworkers reported the self-assembly of CB7•ferrocenyl

[a] *P. Picchetti, N. M. Kumar, P. Gruhs, F. Biedermann*
Institute of Nanotechnology (INT) Karlsruhe Institute of Technology (KIT)
Kaiserstrasse 12, 76131 Karlsruhe, Germany
E-mail: frank.biedermann@kit.edu
pierre.picchetti@kit.edu

[b] *M. V. Balli, L. Prodi*
Department of Chemistry "Giacomo Ciamician", Università degli Studi di Bologna,
Via Selmi 2, Bologna, 40126, Italy

[c] *S. Baker*
Department of Chemistry, University of Victoria
3800 Finnerty Rd., Victoria, BC V8P 5 C2 (Canada)
and
Centre for Advanced Materials and Related Technology (CAMTEC)
University of Victoria
3800 Finnerty Rd., Victoria, BC V8 W 2Y2 (Canada)

Supporting information for this article is available on the WWW under https://doi.org/10.1002/anse.202400025

Research Article
doi.org/10.1002/anse.202400025

Chemistry Europe
European Chemical Societies Publishing

alkane thiolate monolayers on gold electrodes and showed the application of such electrodes to detect quaternary ammonium or thiazole compounds via potentiometric methods.[15] Recently, our group has developed an electrochemical detection method with a CB7-based chemosensor using a platinum complex as the electroactive indicator for detecting electro-inactive drugs in buffered solutions and urine.[16] Apart from these examples, CB*n* have been used to functionalize electrode surfaces to capture and accumulate electroactive biomolecules at this interface, mainly to improve the sensitivity and selectivity of electrochemical detection.[17]

In this study, we present the first example of a CB7-based and unimolecular chemosensor that enables the simultaneous use of fluorescent and electrochemical signals for drug detection. The assay is compatible with plate readers and screen-printed electrodes (SPEs) and can be performed in minutes. Furthermore, this work also highlights the potential of chemosensors for future multimodal assays for the rapid detection of analytes at the point of care.

Results and Discussion

Fluorescence and Electrochemical Changes of CB7-NBD in the Presence of the Analyte TMA

Initially, we focused on the redox behavior of bimolecular CB7-based chemosensors with fluorescent dyes such as berberine chloride and neutral red in aqueous buffers to identify examples with potential dual readout features. Unfortunately, these examples provided unsuitable or suboptimal electrochemical response features for our purposes (Further details and the electrochemical reaction can be found in Figure S1).

Consequently, we focused our attention on the unimolecular cucurbit[7]uril-linked 4-chloro-7-nitrobenzofurazan (CB7-NBD) chemosensor,[12b] in which the NBD indicator is covalently tethered to the outer rim of CB7 via a flexible tetraethylene glycol-based linker (Figure 1a). Notably, this chemosensor, developed by our group, exhibits dilution-stable and salt-adaptive binding properties, enabling the differentiated detection of bioactive analytes.[12b] We were pleased to find that the nitrobenzofurazan moiety in CB7-NBD exhibits a distinct oxidation potential peak (vide infra) within the water window (0–1.2 V), making it suitable for applications in aqueous systems. This property formed the basis for the subsequent development of a dual readout indicator displacement assay (drIDA) utilizing CB7-NBD, as shown in Figure 1a.

As mentioned above, we investigated the electrochemical properties of CB7-NBD by differential pulse voltammetry (DPV, see Supporting Information for further details) since the aromatic Ar-NH- moiety of NBD can be electrochemically oxidized within the electrochemical window of water.[18] To this end, a CB7-NBD solution (25 μM) in phosphate-buffered saline (PBS, 1X, pH = 7.4) was analyzed in the absence or presence of 1 equivalent of N,N,N-trimethyl-1-adamantylammonium hydroxide (TMA; log $K_{a,CB7} = 12.2$).[19]

As shown in Figure 1b, the addition of TMA to the CB7-NBD solution leads to an increase in the observed current density peak (j_{ox}) at an oxidation potential (E_{ox}) of 0.76 V. This increase is due to the facilitated electrochemical oxidation of unbound NBD following its displacement from the CB7 cavity by the competitive binder TMA.[14a,20] Further evidence of the modified

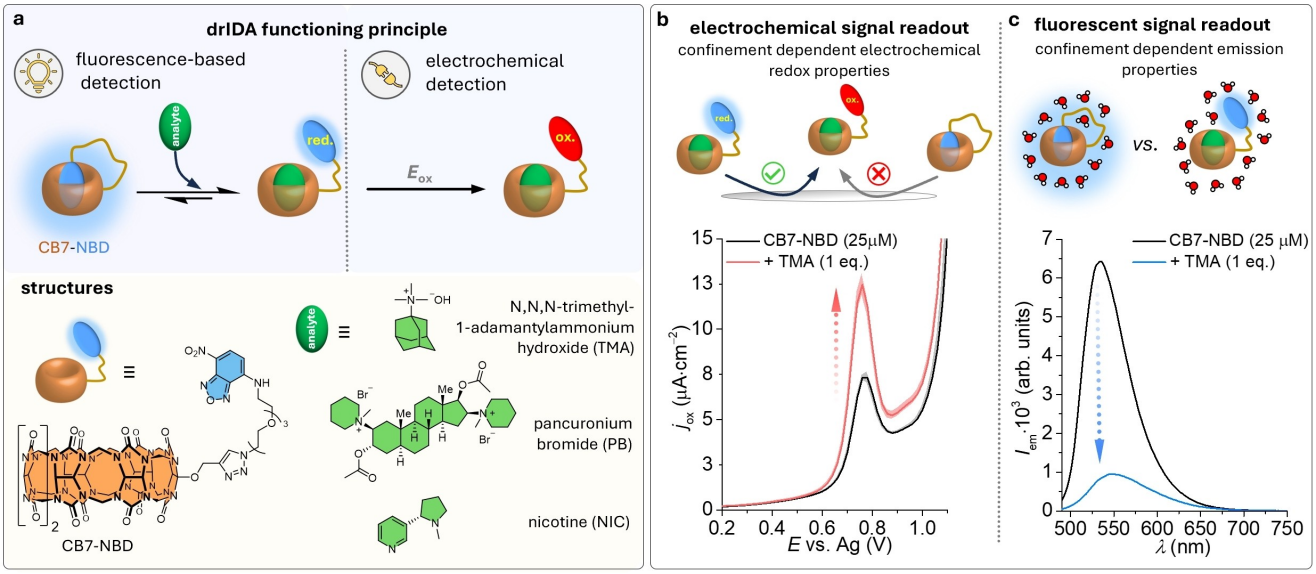

Figure 1. (a) Schematic representation of the dual–fluorescent and electrochemical-detection of drugs with CB7-NBD in the drIDA assay. Shown are also the chemical structure of CB7-NBD and the analytes tested. For better visualization, the Na^+ cation bound to the opposite portal where NBD enters the macrocycles has been omitted from the cartoons.[12b] (b) DPV and (c) fluorescence analysis of CB7-NBD in the absence and presence of 1 equivalent of TMA (in 1X PBS at pH = 7.4; $c_{CB7\text{-}NBD} = 25$ μM). When residing within the cavity of CB7, the fluorescence of NBD is significantly enhanced due to confinement effects. However, its displacement from the CB7 cavity leads to a decrease in emission intensity, while at the same time electrochemical oxidation of the indicator at the anode surface is facilitated, as shown by an increased j_{ox}. The average j_{ox} with the corresponding standard deviation (σ) was calculated from three independent measurements.

oxidation behavior comes from the observed changes in E_{ox}. In the absence of TMA, the E_{ox} for CB7-NBD is observed at 0.76 V. However, in the presence of TMA, this peak shifts to a lower value by 23 mV, indicating the displacement effect of TMA and the facilitated oxidation of NBD when it is not complexed with CB7, as shown in Figure 2a. These results are consistent with previous results in the electrochemical study of host-guest complexation of ferrocene with CB7.[14a] However, the significant changes in j_{ox} can be attributed to the ion pairing between the positively charged [CB7-NBD⊃TMA]$^+$ complex and the phosphate anions from the buffer solution.[21] The migration of these [CB7-NBD⊃analyte]$^+$ species is larger than the one of the non-charged CB7-NBD (see Figure S2).

A concentration-dependent increase in j_{ox} was observed with increasing TMA concentration (0–100 μM; Figure S3), indicating that together with the fluorescence response observed for TMA, a drIDA can be set up for both fluorescent and electrochemical drug detection using CB7-NBD. Cyclic voltammetry (CV) showed that the electrochemical oxidation of CB7-NBD is irreversible (Figure 2b), and studies at different scan rates indicate a diffusion-driven process at the electrode both with and without TMA (Figure 2c).

The optical response of CB7-NBD ($c_{CB7\text{-}NBD}$ = 25 μM) in the absence and presence of 1 equivalent of TMA was tested in PBS (1X, pH = 7.4). As shown in Figure 1c, the fluorescence intensity (I_{em}, λ_{ex} = 470 nm) of CB7-NBD decreases significantly (14-fold) after the addition of TMA, while the absorbance spectrum shows only a slight change (Figure S4a). Fluorescence titration experiments with TMA (0–100 μM) further support the NBD displacement from the CB7 cavity (see Figure S4b). The observed decrease in fluorescence intensity is attributed to the energy dissipation of the excited state of the non-complexed NBD, which is located outside the macrocyclic cavity where confinement effects are absent.[12b,22]

Development of the drIDA

Before we set out to detect biologically relevant analytes, we first focused on establishing a functional protocol for a drIDA using the CB7-NBD system. We used a fluorescence plate reader for optical detection purposes and performed DPV analyses with a portable device equipped with SPEs – both device types that are commercially available and commonly used in research and industrial laboratories (Figure 3a). The possibility of using one chemosensor for both fluorescence and electrochemical detection is particularly interesting in the context of miniaturizable devices that require only minimal sensor components,[23] which in our case is given by the sole presence of the CB7-NBD.

For detecting TMA (in 1X PBS, pH = 7.4) through the drIDA (Figure 3b), analyte was added ($c_{final,TMA}$ = 0–100 μM) to the CB7-NBD ($c_{final,CB7\text{-}NBD}$ = 25 μM) in a well of a 96-well plate (V_{final} = 200 μL), mixed briefly and left to stand for 3 min to ensure equilibration. Subsequently, the emission intensities (λ_{ex} = 470 nm, λ_{em} = 530 nm) were recorded (see Supporting Information for further details). After completion of the fluorescence measurement, an aliquot (50 μL) of the sample in the well was subjected to DPV measurements. For this purpose, the solution was dropped onto the SPE, and DPV analysis was performed, which was completed on a second-time scale (see Supporting Information for further details).

The results of fluorescence and DPV analysis using our drIDA in response to TMA are shown in Figure 3c. In fluorescence mode, the emission intensity of NBD decreases with increasing TMA concentration until the equivalence point is reached – the point at which the molar amount of NBD is equal to that of TMA. On the other hand, the DPV analysis shows an increase in j_{ox} at E_{ox} = 0.76 V with increasing TMA concentration up to the equivalence point.

The limit of detection (LOD) for TMA using the fluorescence method was calculated to be 1.1 μM, while the DPV measurement resulted in a LOD of 0.1 μM (Figure S5; see Supporting Information for further details). Based on these positive results, we next tested the drIDA to detect drugs.

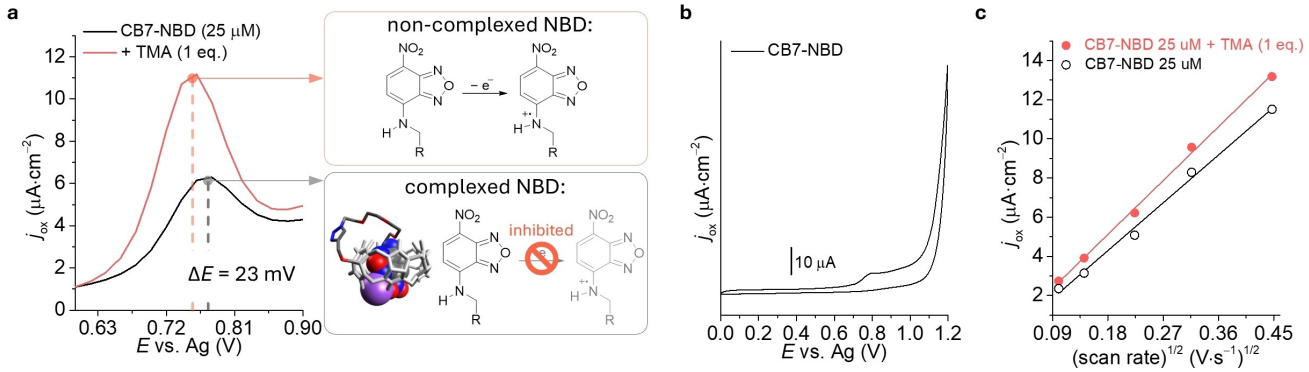

Figure 2. (a) DPV analysis of CB7-NBD (25 μM, in 1X PBS, pH = 7.4) without and after the addition of 1 equivalent of TMA. Shown are the structures of CB7-NBD•Na$^+$ (the bound Na$^+$ cation is represented by the purple sphere) in its complexed form, as well as the electrochemical oxidation reaction for NBD. The CB7-NBD•Na$^+$ structure was adapted with permission from ref. [12b]. Copyright 2023, American Chemical Society. (b) CV spectrum of CB7-NBD (25 μM) in PBS (1X, pH = 7.4). (c) The linear dependence of j_{ox} at E_{ox} = 0.76 V as a function of the square root of the scan rate of CB7-NBD (25 μM) with and without the presence of TMA (1 equivalent) in PBS (1X, pH = 7.4). The scan rates of 10, 20, 50, 100, and 200 mV·s^{-1} were used.

Research Article
doi.org/10.1002/anse.202400025

Chemistry Europe
European Chemical Societies Publishing

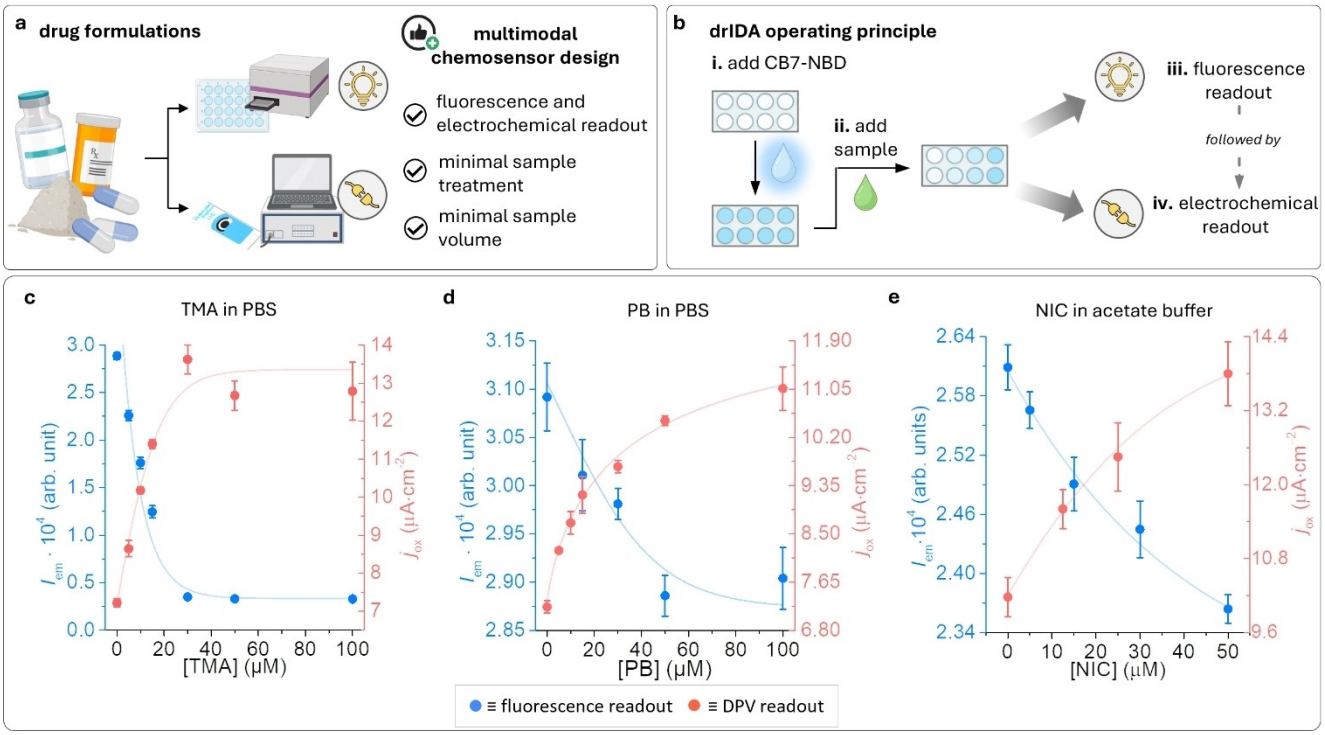

Figure 3. (a) Schematic representation of the dual-readout detection possibilities of drugs with the drIDA, which require minimal sample volumes and pretreatment steps. (b) Schematic representation of the operating principle of the drIDA. (c-e) Fluorescence (blue traces) and DPV response curves (red traces) for the detection of TMA, PB, and NIC with the drIDA ($c_{CB7\text{-}NBD}$ = 50 μM; fluorescence readout: λ_{ex} = 470 nm, λ_{em} = 530 nm). The change in j_{ox} at E_{ox} = 0.76 V was used for the detection of TMA and PB. For the detection of NIC, the change in j_{ox} at E_{ox} = 0.85 V was used. The average I_{em} and j_{ox} with the corresponding standard deviation (σ) were calculated from three independent measurements.

Detection of Pancuronium Bromide and Nicotine with the drIDA

The drIDA procedure was used for the detection of drugs (Figure 1a), such as pancuronium bromide (PB, log K_a = 5.1 for the 1:1 and log $K_{a,CB7}$ = 10.2 for the 2:1 CB7:PB complex)[24] and nicotine (NIC, log $K_{a,CB7}$ = 2.5 for the 1:1 complex measured in sodium acetate buffer at pH = 4.7).[25] The detection of PB, a steroid-based muscle relaxant, and NIC, a highly addictive alkaloid, is of importance for several reasons. First, on-site detection of PB is critical to detecting cases of improper anesthesia or intoxication at crime scenes, as PB is used by criminals to immobilize their victims.[26] Secondly, nicotine, which is normally found in tobacco products, has become a growing problem as the number of poisoning cases increased, some of which were fatal.[27] This rise is due to the popularity of e-cigarettes and other synthetic products such as concentrated liquid nicotine. State-of-the-art detection for these drugs relies exclusively on time-consuming and costly HPLC-based methods.[28]

Our detection assay was performed in buffered solutions to mimic the salt-rich medium of the illegal drug formulations. We increased the concentration of CB7-NBD in the drIDA drug detection assay to 50 μM, as lower concentrations resulted in a suboptimal signal-to-noise ratio because the drugs analyzed have a lower binding affinity to CB7. The results obtained for the detection of PB (in 1X PBS, pH = 7.4) are presented in Figure 3d and Figure S6. As was anticipated, a PB-dependent decrease in fluorescence intensity and a corresponding increase in j_{ox} at E_{ox} = 0.76 V were observed. Job plot analysis (Figure S7) suggests that CB7-NBD exhibits 1:1 binding stoichiometry (CB7-NBD:PB) with this analyte and 2:1 binding, previously reported, is not observed.[24] The steric hindrance and size of the floppy NBD tetraethylene glycol tail most likely prevents the effective binding of a second CB7-NBD to PB.

It is important to note that PB does not display a significant redox peak within the electrochemical window where the DPV analysis was conducted, as was described in our prior work.[16] The linear response curve was used to calculate the LODs for the detection of PB, which was calculated to be 28.6 μM and 1.8 μM for fluorescence- and DPV-based analysis, respectively (Figure 4a and b; see Supporting Information for further details). To detect NIC, the drIDA assay was performed in acetate buffer (0.1 M, pH = 3.3). This adjustment ensures that the nicotine is protonated at its pyrrolidinyl moiety and substantially protonated also at its pyridinyl moiety ($pK_{a,\ pyrrolidinyl}$ = 8.1; $pK_{a,pyridinyl}$ = 3.4).[29] In its protonated state, NIC exhibits a significantly reduced redox peak current at E_{ox} = 0.85 V at which NBD is oxidized in an acetate buffer (Figure S8). With this adaptation, detection of NIC with the drIDA (Figure 3e and Figure S9) in acetate buffer becomes possible compared to PBS buffer at pH = 7.4, where detection is difficult due to the background signal of NIC itself (see Figure S9). The LOD for the detection of NIC was derived from the linear response, which was calculated

Research Article
doi.org/10.1002/anse.202400025

Chemistry Europe
European Chemical Societies Publishing

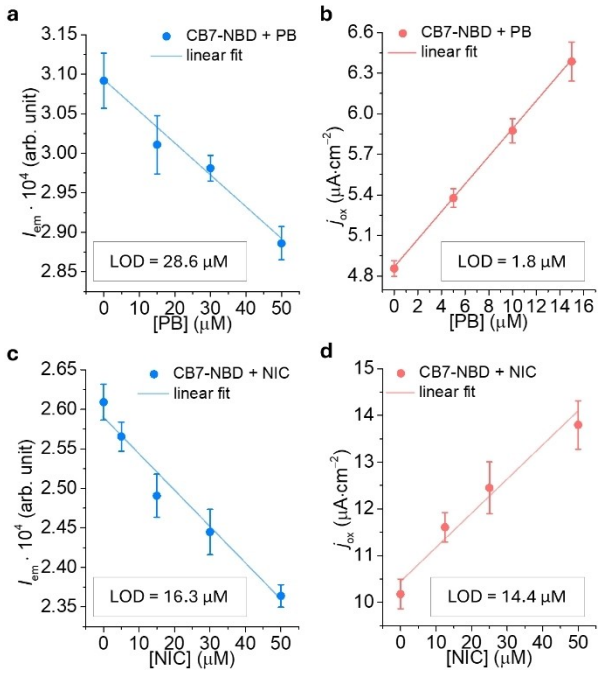

Figure 4. Linear drIDA response curves for PB in the (a) fluorescence and (b) DPV detection mode. The linear regime of the drIDA response curves for NIC in the (c) fluorescence and (d) DPV detection mode. The average I_{em} and j_{ox} with the corresponding standard deviation (σ) were calculated from three independent measurements.

to be 16.3 μM for the fluorescence-based detection method and 14.4 μM for the DPV-based detection method (Figure 4c and d).

The change in emission intensities was less pronounced for PB and NIC detection compared to TMA. This observation derives from the formation of a dual-inclusion complex, as described in our previous work,[12b] wherein the NBD dyes are not fully exposed to water. Nevertheless, the observed decreased fluorescence intensity is sufficient for the detection purposes. Regarding the fluorescence-based detection of NIC, the onset of emission intensity for CB7-NBD starts at slightly lower values than those observed for the detection of TMA or PB (Figure 4 and Figure S10). This is because at pH = 3.3, which we utilized for detecting NIC, hydronium ions compete with NBD for binding to CB7, thereby slightly shifting the equilibrium towards the unbound state of the reporter.[35] It is also worth noting that none of the analytes displayed significant absorbance at the excitation wavelength used for CB7-NBD, as shown in Figure S11.

drIDA Performance

Reflected in Table 1, the comparative performance of chemosensors for PB and NIC detection illustrates the capabilities of the drIDA system. Operable in aqueous media, drIDA distinguishes itself by offering rapid fluorescent and electrochemical signal readout which is a noteworthy improvement on the extended assay times typical of HPLC methods. It merits attention that the system's analytical efficiency is achieved with relatively low sample volumes: 200 μL for fluorescence and 50 μL for DPV, underscoring its practical applicability in streamlined chemical investigations.

We have used commercially available and common fluorescent and electrochemical devices used in both research and industrial laboratories. In particular, we used SPEs, without chemical modification steps, that are widely used for detection purposes.[36] Regarding the concentration range for drug detection, it is important to underline that illicit drug formulations contain concentrations of PB (> 100 μM)[37] and NIC (> 135 μM),[38] which are far above the LODs obtained with drIDA. We would like to point out that the CB7-NBD concentration used in this study was specifically chosen to prevent aggregation and avoid potential internal filter effects. Therefore, real samples that might contain higher concentrations of PB or NIC can be diluted and appropriate calibration curves in the micromolar range should be established before analysis. Nonetheless, the derived LOD values should be regarded as approximate values since the supramolecular host-guest interactions do not follow linear relationships. Moreover, it is important to acknowledge that the detection capabilities of drIDA could be adversely affected by the concurrent presence of other amine-bearing compounds like amantadine, which possess a high affinity for CB7.

Our drIDA can detect PB and NIC in aqueous media or saline buffers, simulating complex scenarios, however, we investigated other potential interferents for our drIDA method. Other organic compounds, including vecuronium bromide (VB, log K_a = 10.7 for the 1:1 complex with CB7),[24] L-phenylalanine (PHE, log K_a = 5.5),[39] creatinine (CRE) and insulin (INS) were tested at levels typically found in beverages or biofluids to assess their potential interference (see Figure 5a).[40] We also tested the chemosensor in a non-diluted sweet drink, i.e. 7 Up.

Figure 5b and c show the changes in I_{em} or j_{ox} compared to CB7-NBD alone. As expected, VB causes significant interference due to its structural similarity to PB, whereas PHE and INS also cause interference, but to a considerably lesser extent (Figure S12). While PHE is a known medium-affinity CB7-binding amino acid, INS deactivates CB*n* chemosensors by phenylalanine-glycine residue binding of this protein.[41]

In non-diluted 7 Up soft drink the CB7-NBD was found to be still active for high-affinity binders such as TMA through fluorescence (Figure S13). The detection of PB in this soft drink via the fluorescence mode was not possible. In both cases, TMA and PB could not be detected via DPV due to the complex composition of the soft drink, which interfered with electrochemical detection.

Future directions involve assessing the drIDA method in biofluids to refine its accuracy and applicability, ensuring its robustness in complex sample matrices.

Conclusions

The drIDA presented in this work represents a novel CB7-based unimolecular chemosensor capable of measuring pancuronium bromide and nicotine at low micromolar concentrations in

Research Article
doi.org/10.1002/anse.202400025

Chemistry Europe
European Chemical Societies Publishing

Table 1. Comparison of different chemosensors for the detection of PB and NIC. AcO: acetate; CD: cyclodextrin; FRA: fraxetin; MB: methylene blue; PBS: phosphate buffered saline; n.a.: not applicable.

analyte	chemosensor	method	conc. range [μM]	LOD [μM]	sample	ref.
pancuronium bromide						
	acyclic CB*n*-type•acridine	absorbance	0.0–460.0	n.a.	phosphate buffer (20 mM, pH = 7.4)	[30]
	CB7⊃Pt-complex	DPV	0.0–200.0	4.3	PBS (5 mM, pH = 7.0)	[16]
	CB7⊃Pt-complex	DPV	0.0–200.0	6.3	urine/PBS (1 : 3 v/v, 5 mM PBS, pH = 7.0)	[16]
	CB7-NBD	DPV	0.0–200.0	1.8	PBS (1X PBS, pH = 7.4)	this work
	CB7-NBD	fluorescence	0.0–200.0	28.6	PBS (1X PBS, pH = 7.4)	this work
nicotine						
	CB7•MB	fluorescence	12.0–48.0	0.3	AcO buffer (50 mM, pH = 4.7)	[25]
	CB7•azobenzene	absorbance	0.0–1500.0	n.a.	acetate buffer (50 mM, pH = 4.7)	[31]
	CD•FRA	fluorescence	10.0–50.0	1.0	water	[32]
	Zn-porphyrin	fluorescence	0.0–3.8	n.a.	toluene	[33]
	Zn-porphyrin	piezoelectric microgravimetry	100.0–1000.0	120.0	AcO buffer/EtOH (1 : 1 v/v,100 mM AcO; pH = 4.2)	[34]
	CB7-NBD	DPV	0.0–200	14.4	AcO buffer (0.1 M, pH = 3.3)	this work
	CB7-NBD	fluorescence	0.0–200	16.3	AcO buffer (0.1 M, pH = 3.3)	this work

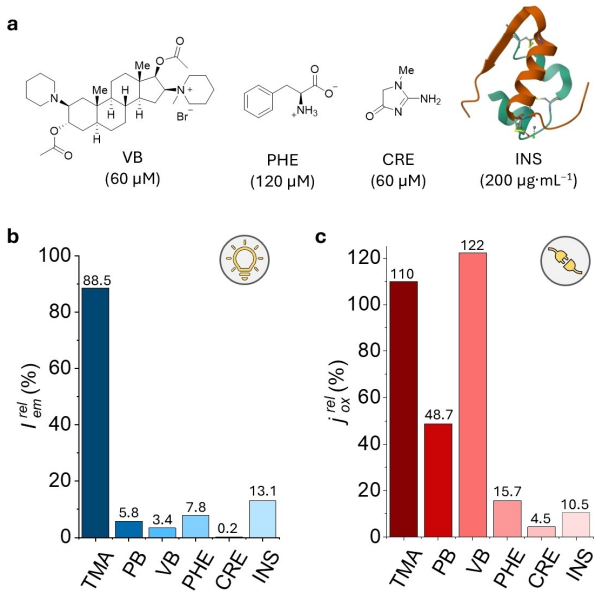

Figure 5. (a) Chemical structures of VB, PHE, CRE and INS and concentrations used to evaluate their response with CB7-NBD. Relative change in signal due to potential interferents compared to the signal of CB7-NBD alone in (b) fluorescence and (c) DPV readout modality. The image for the human insulin structure was adapted with permission from the RCSB Protein Data Bank (RCSB PDB).

aqueous media in two ways – fluorescently and electrochemically. Its design is compatible with standard fluorescence plate readers and commercially available electrochemical devices. In addition, the use of disposable and commercially available screen-printed electrodes facilitates analysis with minimal sample volumes and enables fast results in less than 5 minutes.

Given the advancements in portable and wearable optical and electrochemical technologies, the drIDA method holds potential for facilitating rapid, cost-effective, and accessible drug detection by non-experts, such as law enforcement personnel, in urgent or remote settings, where HPLC-based methods may not be applicable.

Supporting Information

Details about instruments, materials, and methods are available in the supporting information. The authors have cited additional references within the Supporting Information.[42][43]

Acknowledgements

N.M.K. acknowledges the German Academic Exchange Service (DAAD) for financial support. P.G., P.P. and F.B. acknowledge the Emmy Noether program of the Deutsche Forschungsgemein-

schaft (BI-1805/2-1) and the European Union's Horizon Europe EIC Pathfinder Open programme "ECLIPSE project" (No. 101046787) for financial support. Acknowledgements Text. S. B. acknowledges the Mitacs RISE-Globalink research internship for financial support. Open Access funding enabled and organized by Projekt DEAL.

Conflict of Interests

The authors declare no conflict of interest.

Data Availability Statement

The data that support the findings of this study are available from the corresponding author upon reasonable request.

Keywords: chemosensor · drug detection · electrochemical detection · fluorescence · multimodal

[1] a) J. M. Lehn, J. P. Sauvage, *J. Am. Chem. Soc.* **1975**, *97*, 6700–6707; b) S. La Cognata, V. Amendola, *Chem. Commun.* **2023**, *59*, 13668–13678.
[2] a) E. Biavardi, C. Tudisco, F. Maffei, E. Dalcanale, *PNAS* **2012**, *109*, 2263–2268; b) E. Biavardi, S. Federici, C. Tudisco, D. Menozzi, C. Massera, A. Sottini, G. G. Condorelli, P. Bergese, E. Dalcanale, *Angew. Chem. Int. Ed.* **2014**, *53*, 9183–9188; c) R. Pinalli, E. Dalcanale, *Acc. Chem. Res.* **2013**, *46*, 399–411; d) W. Zhang, R. J. Hooley, *Acc. Chem. Res.* **2022**, *55*, 1035–1046.
[3] a) C. D. Gutsche, R. Muthukrishnan, *J. Org. Chem.* **1978**, *43*, 4905–4906; b) F. Sansone, L. Baldini, A. Casnati, R. Ungaro, *New J. Chem.* **2010**, *34*, 2715–2728; c) A. J. Selinger, N. A. Cavallin, A. Yanai, I. Birol, F. Hof, *Angew. Chem. Int. Ed.* **2022**, *61*, e202113235.
[4] a) O. Tomoki, K. Suguru, F. Shuhei, Y. Tada-aki, N. Yoshiaki, *J. Am. Chem. Soc.* **2008**, *130*, 5022–5023; b) Y. Li, J. Wen, J. Li, Z. Wu, W. Li, K. Yang, *ACS Sens.* **2021**, *6*, 3882–3897.
[5] a) W. A. Freeman, W. L. Mock, N. Y. Shih, *J. Am. Chem. Soc.* **1981**, *103*, 7367–7368; b) J. Kim, I.-S. Jung, S.-Y. Kim, E. Lee, J.-K. Kang, S. Sakamoto, K. Yamaguchi, K. Kim, *J. Am. Chem. Soc.* **2000**, *122*, 540–541; c) S. J. Barrow, S. Kasera, M. J. Rowland, J. del Barrio, O. A. Scherman, *Chem. Rev.* **2015**, *115*, 12320–12406.
[6] a) R. Pinalli, A. Pedrini, E. Dalcanale, *Chem. Soc. Rev.* **2018**, *47*, 7006–7026; b) J. Krämer, R. Kang, L. M. Grimm, L. De Cola, P. Picchetti, F. Biedermann, *Chem. Rev.* **2022**, *122*, 3459–3636.
[7] F. Biedermann, V. D. Uzunova, O. A. Scherman, W. M. Nau, A. De Simone, *J. Am. Chem. Soc.* **2012**, *134*, 15318–15323.
[8] a) A. Praetorius, D. M. Bailey, T. Schwarzlose, W. M. Nau, *Org. Lett.* **2008**, *10*, 4089–4092; b) A. C. Sedgwick, J. T. Brewster, T. Wu, X. Feng, S. D. Bull, X. Qian, J. L. Sessler, T. D. James, E. V. Anslyn, X. Sun, *Chem. Soc. Rev.* **2021**, *50*, 9–38.
[9] a) A. Hennig, H. Bakirci, W. M. Nau, *Nat. Methods* **2007**, *4*, 629–632; b) C. P. Carvalho, R. Ferreira, J. P. Da Silva, U. Pischel, *Supramol. Chem.* **2013**, *25*, 92–100; c) A. I. Lazar, F. Biedermann, K. R. Mustafina, K. I. Assaf, A. Hennig, W. M. Nau, *J. Am. Chem. Soc.* **2016**, *138*, 13022–13029; d) X. Lu, L. Isaacs, *Angew. Chem. Int. Ed.* **2016**, *55*, 8076–8080; e) Q. Bai, S. Zhang, H. Chen, T. Sun, C. Redshaw, J. X. Zhang, X. L. Ni, G. Wei, Z. Tao, *ChemistrySelect* **2017**, *2*, 2569–2573; f) M. Xu, S. P. Kelley, T. E. Glass, *Angew. Chem. Int. Ed.* **2018**, *57*, 12741–12744; g) S. Sinn, E. Spuling, S. Bräse, F. Biedermann, *Chem. Sci.* **2019**, *10*, 6584–6593; h) J. Jiménez, S. Blasco, E. Blanco, P. Atienzar, M. del Pozo, C. Quintana, *ChemistrySelect* **2019**, *4*, 7036–7041; i) D.-A. Xu, Q.-Y. Zhou, X. Dai, X.-K. Ma, Y.-M. Zhang, X. Xu, Y. Liu, *Chin. Chem. Lett.* **2022**, *33*, 851–854; j) N. Das Saha, S. Pradhan, R. Sasmal, A. Sarkar, C. M. Berac, J. C. Kolsch, M. Pahwa, S. Show, Y. Rozenholc, Z. Topcu, V. Alessandrini, J. Guibourdenche, V. Tsatsaris, N. Gagey-Eilstein, S. S. Agasti, *J. Am. Chem. Soc.* **2022**, *144*, 14363–14379; k) R. Jiang, M. Nilam, A. Hennig, W. M. Nau, *Adv. Mater.* **2024**, *36*, e2306922.
[10] a) K. L. Kim, G. Sung, J. Sim, J. Murray, M. Li, A. Lee, A. Shrinidhi, K. M. Park, K. Kim, *Nat. Commun.* **2018**, *9*, 1712; b) R. Sasmal, N. Das Saha, F. Schueder, D. Joshi, V. Sheeba, R. Jungmann, S. S. Agasti, *Chem. Commun.* **2019**, *55*, 14430–14433; c) C. Wang, Y. H. Liu, Y. Liu, *Small* **2022**, *18*, e2201821; d) B. D. Gates, J. B. Vyletel, L. Zou, M. J. Webber, *Bioconjugate Chem.* **2022**, *33*, 2262–2268.
[11] J. Krämer, L. M. Grimm, C. Zhong, M. Hirtz, F. Biedermann, *Nat. Commun.* **2023**, *14*, 518.
[12] a) C. Hu, L. Grimm, A. Prabodh, A. Baksi, A. Siennicka, P. A. Levkin, M. M. Kappes, F. Biedermann, *Chem. Sci.* **2020**, *11*, 11142–11153; b) C. Hu, T. Jochmann, P. Chakraborty, M. Neumaier, P. A. Levkin, M. M. Kappes, F. Biedermann, *J. Am. Chem. Soc.* **2022**, *144*, 13084–13095.
[13] a) M. Mayer, A. J. Baeumner, *Chem. Rev.* **2019**, *119*, 7996–8027; b) H. Teymourian, M. Parrilla, J. R. Sempionatto, N. F. Montiel, A. Barfidokht, R. Van Echelpoel, K. De Wael, J. Wang, *ACS Sens.* **2020**, *5*, 2679–2700; c) Z. Yang, T. Albrow-Owen, W. Cai, T. Hasan, *Science* **2021**, *371*, 480; d) H. C. Ates, P. Q. Nguyen, L. Gonzalez-Macia, E. Morales-Narváez, F. Guder, J. J. Collins, C. Dincer, *Nat. Rev. Mater.* **2022**, *7*, 887–907; e) S. R. S. Pour, D. Calabria, A. Emamiamin, E. Lazzarini, A. Pace, M. Guardigli, M. Zangheri, M. Mirasoli, *Chemosensors* **2023**, *11*, 546.
[14] a) W. S. Jeon, K. Moon, S. H. Park, H. Chun, Y. H. Ko, J. Y. Lee, E. S. Lee, S. Samal, N. Selvapalam, M. V. Rekharsky, V. Sindelar, D. Sobransingh, Y. Inoue, A. E. Kaifer, K. Kim, *J. Am. Chem. Soc.* **2005**, *127*, 12984–12989; b) M. H. Tootoonchi, S. Yi, A. E. Kaifer, *J. Am. Chem. Soc.* **2013**, *135*, 10804–10809.
[15] a) L. Qi, R. Wang, H. Z. Yu, *Anal. Chem.* **2020**, *92*, 2168–2175; b) L. Qi, R. Wang, H.-Z. Yu, *Acc. Mater. Res.* **2023**, *4*, 457–466.
[16] N. M. Kumar, P. Gruhs, A. Casini, F. Biedermann, G. Moreno-Alcántar, P. Picchetti, *ACS Sens.* **2023**, *8*, 2525–2532.
[17] a) M. del Pozo, J. Mejías, P. Hernández, C. Quintana, *Sens. Actuators B* **2014**, *193*, 62–69; b) É. V. d'Astous, P. Dauphin-Ducharme, *Curr. Opin. Electrochem.* **2022**, *34*, 101029; c) Y. Wang, L. Ding, H. Yu, F. Liang, *Chin. Chem. Lett.* **2022**, *33*, 283–287; d) T. Ma, S. Chang, J. He, F. Liang, *Chem. Commun.* **2023**, *60*, 150–167; e) Y. Jang, M. Jang, H. Kim, S. J. Lee, E. Jin, J. Y. Koo, I.-C. Hwang, Y. Kim, Y. H. Ko, I. Hwang, J. H. Oh, K. Kim, *Chem. Commun.* **2017**, *3*, 641–651.
[18] H. Raissi, I. Chérif, I. Aribi, H. Ayachi, A. Haj Said, S. Ayachi, T. Boubaker, *Chem. Pap.* **2022**, *76*, 4059–4080.
[19] S. Liu, C. Ruspic, P. Mukhopadhyay, S. Chakrabarti, P. Y. Zavalij, L. Isaacs, *J. Am. Chem. Soc.* **2005**, *127*, 15959–15967.
[20] C. Yao, H. Lin, B. Daly, Y. Xu, W. Singh, H. Q. N. Gunaratne, W. R. Browne, S. E. J. Bell, P. Nockemann, M. Huang, P. Kavanagh, A. P. de Silva, *J. Am. Chem. Soc.* **2022**, *144*, 4977–4988.
[21] a) J. J. Watkins, H. S. White, *Langmuir* **2004**, *20*, 5474–5483; b) J.-M. Savéant, *J. Phys. Chem. B* **2001**, *105*, 8995–9001.
[22] a) R. N. Dsouza, U. Pischel, W. M. Nau, *Chem. Rev.* **2011**, *111*, 7941–7980; b) H. Nie, Z. Wei, X. L. Ni, Y. Liu, *Chem. Rev.* **2022**, *122*, 9032–9077.
[23] a) J. Matthews, J. Kim, W. H. Yeo, *Anal. Sens.* **2022**, *3*, e202200062; b) J. F. Hernández-Rodríguez, D. Rojas, A. Escarpa, *Anal. Chem.* **2021**, *93*, 167–183; c) A. F. Coskun, S. N. Topkaya, A. K. Yetisen, A. E. Cetin, *Adv. Opt. Mater.* **2019**, *7*, 1801109; d) D. Sen, R. A. Lazenby, *Anal. Sens.* **2023**, e202300047; e) B. D. Mansuriya, Z. Altintas, *Fundamentals of Sensor Technology: 24 - Screen-printed electrochemical sensor platforms*, Woodhead Publishing, Elsevier, **2023**;p. 745.
[24] M. A. Gamal-Eldin, D. H. Macartney, *Can. J. Chem.* **2014**, *92*, 243–249.
[25] Y. Zhou, H. Yu, L. Zhang, H. Xu, L. Wu, J. Sun, L. Wang, *Microchim. Acta* **2008**, *164*, 63–68.
[26] R. E. Johnstone, R. L. Katz, T. H. Stanley, *Anesthesiology* **2011**, *114*, 713–716.
[27] a) A. Miller, *CMAJ* **2014**, *186*, E367; b) B. Wang, S. Liu, A. Persoskie, *Clin. Toxicol.* **2020**, *58*, 488–494.
[28] a) P. L. García, F. P. Gomes, M. I. R. M. Santoro, E. R. M. Kedor-Hackmann, *Anal. Lett.* **2008**, *41*, 1895–1908; b) D. Palazzolo, J. M. Nelson, Z. Hudson, *Int. J. Environ. Res. Public Health* **2019**, *16*, 3015.
[29] V. V. Gholap, L. Kosmider, L. Golshahi, M. S. Halquista, *Expert Opin. Drug Delivery* **2020**, *17*, 1727–1736.
[30] D. Ma, B. Zhang, U. Hoffmann, M. G. Sundrup, M. Eikermann, L. Isaacs, *Angew. Chem. Int. Ed.* **2012**, *51*, 11358–11362.
[31] J. Wu, L. Isaacs, *Chem. Eur. J.* **2009**, *15*, 11675–11680.
[32] Y. H. Yang, Z. Zhang, Q. L. Bao, F. Zhao, M. K. Yang, X. Tao, Y. Chen, J. T. Zhang, L. J. Yang, *Carbohydr. Polym.* **2024**, *327*, 121624.
[33] G. R. Deviprasad, F. D'Souza, *Chem. Commun.* **2000**, 1915–1916.
[34] K. Noworyta, W. Kutner, C. A. Wijesinghe, S. G. Srour, F. D'Souza, *Anal. Chem.* **2012**, *84*, 2154–2163.

[35] S. Zhang, L. Grimm, Z. Miskolczy, L. Biczók, F. Biedermann, W. M. Nau, *Chem. Commun.* **2019**, *55*, 14131–14134.
[36] a) I. Vasilescu, S. A. V. Eremia, R. Penu, C. Albu, A. Radoi, S. C. Litescu, G.-L. Radu, *RSC Adv.* **2015**, *5*, 261–268; b) S. Søpstad, E. A. Johannessen, F. Seland, K. Imenes, *Electrochim. Acta* **2018**, *287*, 29–36; c) L. Patinglag, M. M. N. Esfahani, K. Ragunathan, P. He, N. J. Brown, S. J. Archibald, N. Pamme, M. D. Tarn, *Analyst* **2020**, *145*, 4920–4930.
[37] C. H. M. Kerskes, K. J. Lusthof, P. G. M. Zweipfenning, J. P. Franke, *J. Anal. Toxicol.* **2002**, *26*, 29–34.
[38] M. R. Peace, T. R. Baird, N. Smith, C. E. Wolf, J. L. Poklis, A. Poklis, *J. Anal. Toxicol.* **2016**, *40*, 403–407.
[39] L. M. Grimm, J. Setiadi, B. Tkachenko, P. R. Schreiner, M. K. Gilson, F. Biedermann, *Chem. Sci.* **2023**, *14*, 11818–11829.
[40] a) M. Cleary, F. Trefz, A. C. Muntau, F. Feillet, F. J. van Spronsen, A. Burlina, A. Bélanger-Quintana, M. Giżewska, C. Gasteyger, E. Bettiol, N. Blau, A. MacDonald, *Mol. Genet. Metab.* **2013**, *110*, 418–423; b) K. van Vliet, E. S. Melis, P. de Blaauw, E. van Dam, R. G. H. J. Maatman, D. Abeln, F. J. van Spronsen, M. R. Heiner-Fokkema, *Nutrients* **2020**, *12*, 1887; c) K. Kashani, M. H. Rosner, M. Ostermann, *Eur. J. Intern. Med.* **2020**, *72*, 9–14.
[41] a) Y.-H. Liu, Y.-M. Zhang, H.-J. Yu, Y. Liu, *Angew. Chem. Int. Ed.* **2021**, *60*, 3870–3880; b) P. Picchetti, A. K. Pearce, S. J. Parkinson, L. M. Grimm, R. K. O'Reilly, F. Biedermann, *Macromolecules* **2024**, *57*, 4062–4071.
[42] a) C. Marquez, F. Huang, W. M. Nau, *IEEE Transactions on NanoBioscience* **2004**, *3*, 39–45; b) A. Prabodh, S. Sinn, L. Grimm, Z. Miskolczy, M. Megyesi, L. Biczók, S. Bräse, F. Biedermann, *Chem. Commun.* **2020**, *56*, 12327–12330.
[43] J. Mohanty, A. C. Bhasikuttan, W. M. Nau, H. Pal, *J. Phys. Chem. B* **2006**, *110*, 5132–5138.

Revised manuscript received: May 28, 2024
Accepted manuscript online: June 5, 2024
Version of record online: ■■, ■■

RESEARCH ARTICLE

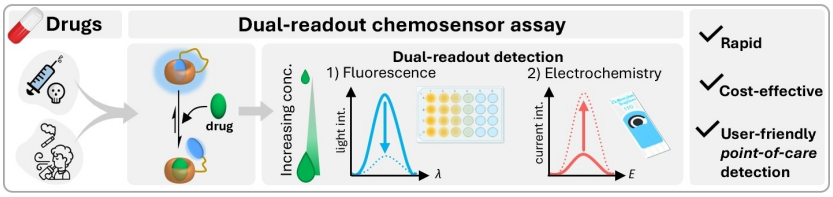

A dual readout chemosensor assay is presented that utilizes a cucurbit[7]uril (CB7)-indicator conjugate for the optical and electrochemical detection of drugs in water. The assay works on the basis that the fluorescence and electrochemical properties of the reporter molecule change when it is engulfed by the CB7 or displaced from its cavity by an analyte. This approach enables the detection of drugs such as pancuronium bromide or nicotine in low micromolar concentrations (0–100 μM).

P. Picchetti, M. V. Balli, S. Baker, N. M. Kumar, P. Gruhs, L. Prodi, F. Biedermann**

1 – 9

Unimolecular Cucurbit[7]uril-Based Indicator Displacement Assay with Dual Signal-Readout for the Detection of Drugs